J Mater Sci (2010) 45:1419–1424
DOI 10.1007/s10853-009-4110-7

LETTER

Controlled synthesis of $MnFe_2O_4$–Ni core–shell nanoparticles

Su-Chul Yang · Cheol-Woo Ahn · Chee-Sung Park · Yaodong Yang · Dwight Viehland · Shashank Priya

Received: 7 October 2009 / Accepted: 4 December 2009 / Published online: 18 December 2009

Introduction

Magnetic nanoparticles have been of significant interest for various applications such as data information storage [1, 2], biomedical drug delivery [3], magnetic resonance imaging [4], and energy harvesting [5] due to their unique characteristics as a function of size. To improve the functionality of magnetic sensors various studies are being conducted on magnetic material–metal composites [6–11]. In this study, we focused on the synthesis of ceramic–metal core–shell particles via an aqueous method as schematically illustrated in Fig. 1a [12]. $MnFe_2O_4$ core particles were synthesized by a solvothermal method, and then Ni shells were coated onto the core particles by ionic interaction between Ni^+ ions and negatively charged $MnFe_2O_4$ particles. The motivation behind the synthesis of nanoparticles is that they could potentially lead to the realization of new type of magnetic field sensors that utilizes thermal detection to quantify the changes in external magnetic field. An oscillating magnetic field in the surrounding will induce eddy current in the conductive shells that could result in the joule heating of the core. Furthermore, the oscillating magnetic field will induce strain in the core due to magnetostriction which will create deformation in the matrix. The result of these two effects will be to create a finite temperature difference with the surrounding. Ceramic–metal core–shell particles are also promising for designing composites that exhibit electromagnetostrictive (EMS) effect where current flowing on conductive shells could induce a magnetic bias in insulating magnetostrictive grains, resulting in an induced strain in the grains through electromagnetoelastic coupling. If a ferroelectric layer is present on top of the metal shell in the configuration ceramic/metal/ceramic, then the strain from magnetostrictive grains will result in generation of electric charge on ferroelectric layer. Sensing can be conducted by monitoring the output electric charge as a function of applied magnetic field. The immediate advantage of such an approach is that the entire EMS effect would be electrically controllable. However, the first and foremost challenge in achieving these effects is to control the thickness of the nickel shell in range of 1–5 nm which are coated on magnetostrictive cores with diameters of few hundred nanometers.

Experimental

First, particles of $MnFe_2O_4$ were synthesized by coprecipitation of Mn^{II} and Fe^{III} ($Mn^{2+}/Fe^{3+} = 0.5$) in ethylene glycol. Staring materials of $MnCl_2{\cdot}4H_2O$ (0.50 g, 2.5 mmol) and $FeCl_3{\cdot}6H_2O$ (1.35 g, 5 mmol) were dissolved in ethylene glycol (40 mL) after which 3.6 g of NaAc and 1.0 g of polyethylene glycol was added to the solution. The mixture was stirred vigorously for 30 min and then sealed in an autoclave. The autoclave was heated to 200 °C for 24 h and slowly cooled to room temperature resulting in the formation of $MnFe_2O_4$ particles. These particles were retrieved, washed several times with ethanol and dried at 60 °C for 6 h. To characterize the magnetic response of individual particles through magnetic force

S.-C. Yang · C.-W. Ahn · C.-S. Park · Y. Yang · D. Viehland · S. Priya (✉)
Department of Materials Science and Engineering,
Center for Energy Harvesting Materials and Systems (CEHMS),
Virginia Polytechnic Institute and State University,
Blacksburg, VA 24061, USA
e-mail: spriya@vt.edu

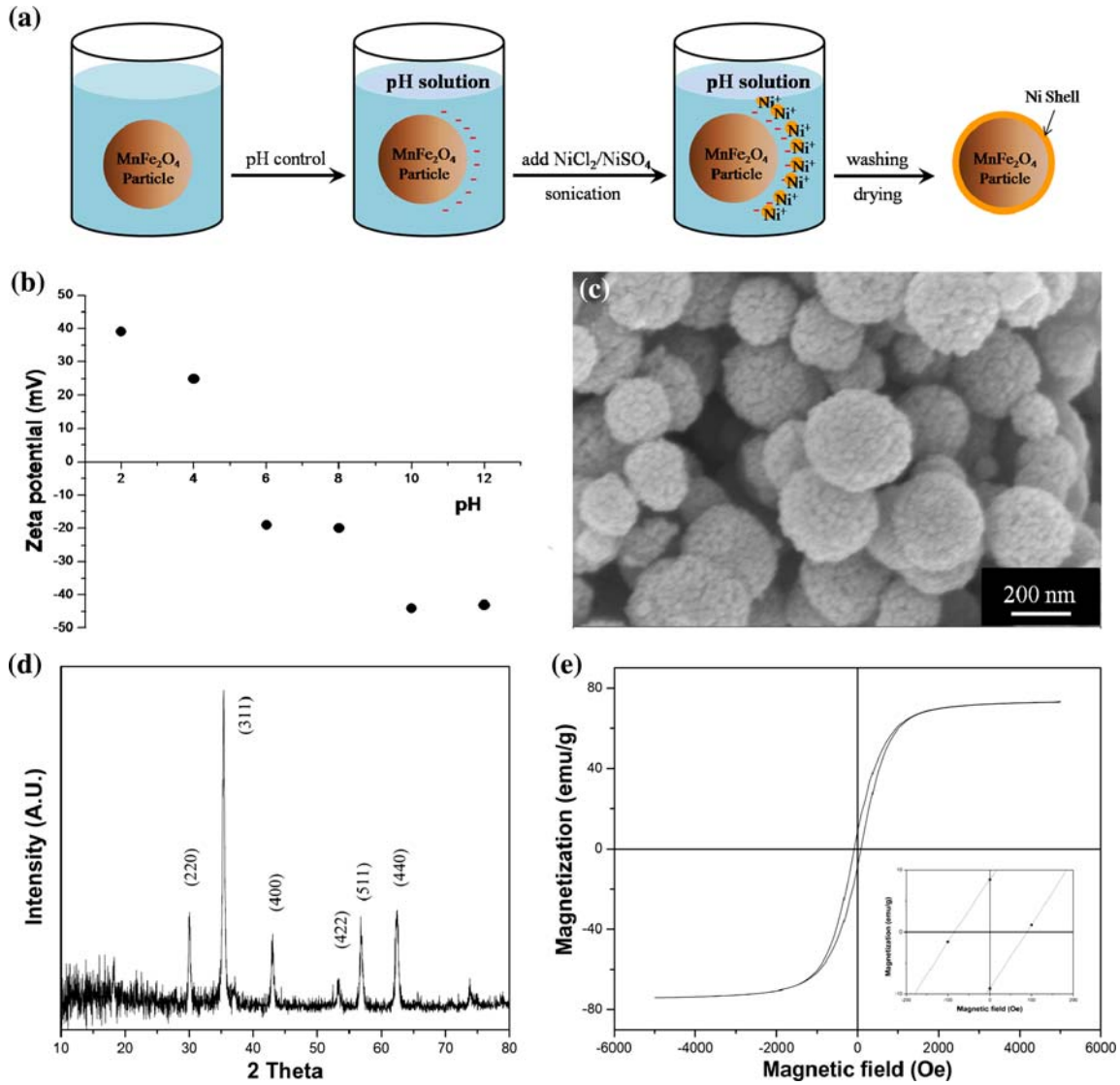

Fig. 1 **a** Schematic diagram of the procedure used to synthesize $MnFe_2O_4$–Ni core–shell particles, **b** Zeta-potentials of $MnFe_2O_4$ particles for $2 \leq pH \leq 12$, **c** SEM image of $MnFe_2O_4$ particles, **d** XRD pattern of $MnFe_2O_4$ particles, and **e** M–H curve of $MnFe_2O_4$ particles

microscopy (MFM), $MnFe_2O_4$ particles were spread on a glass substrate by repeated dipping. For this purpose, 0.1 mg of $MnFe_2O_4$ was added into 15 mL ethanol and the colloidal solution was sonicated for 10 min. After which a glass substrate was vertically dipped five times in this colloidal ethanol solution and subsequently dried at room temperature.

Next, $MnFe_2O_4$–Ni composite core–shell particles were synthesized by an aqueous method as illustrated in Fig. 1a. One milligram of $MnFe_2O_4$ was added into 15 mL of aqueous solution with pH = 10: where the pH magnitude was adjusted by adding HNO_3 or TEAOH (tetraethylammonium hydroxide). Particles of $MnFe_2O_4$ suspended in the aqueous solution (pH = 10) possessed a negative surface potential of −40 mV, as shown in Fig. 1b. The raw materials of 0.08 g of $NiCl_2{\cdot}6H_2O$ and 0.23 g of $NiSO_4{\cdot}6H_2O$ were added to the solution, and the mixture was then sonicated for 10 min, resulting in the formation of $MnFe_2O_4$-Ni core–shell particles. During this step, the Ni^+ ions dissociated in the aqueous solutions, and subsequently were coated onto the negatively charged $MnFe_2O_4$ particles. The $MnFe_2O_4$–Ni core–shell particles were washed several times with distilled water and methanol, and then dried at room temperature.

Structural phase analysis of the $MnFe_2O_4$ particles was done by X-ray diffraction (D/MAX-2500, Rigaku). Magnetic properties were measured by magnetic force microscopy or MFM (Vecoo DI 3100a) and a vibrating

sample magnetometer (VSM 7304, Lake Shore Cryotronics). The zeta-potential of the aqueous solutions was measured by a Zetasizer Nano (Malvern). The shell morphology and Ni concentration of the $MnFe_2O_4$-Ni core–shell particles were characterized by a field emission scanning electron microscope (FE-SEM, LEO/Zeiss 1550, Zeiss), in conjunction with energy dispersive spectroscopy (EDS). Detailed structural and microstructural analyses of the synthesized particles were performed by a high-resolution transmission electron microscopy (HRTEM, Titan 300, FEI).

Results and discussion

Figure 1c shows the morphology of the $MnFe_2O_4$ particles synthesized by the solvothermal method. The particles had a high density with a mean size of about 200 nm. These $MnFe_2O_4$ particles were formed by agglomeration of primary nanoparticles with a mean diameter of 15 nm. Phase formation of $MnFe_2O_4$ was confirmed by XRD, as shown in Fig. 1d. No measureable trace of any secondary phase was found in the XRD pattern. At room temperature, the M–H curves for these $MnFe_2O_4$ particles exhibited a saturation magnetization of 74 emu/g and a coercivity of 89 Oe, as shown in Fig. 1e. Figure 2, further confirms that synthesized individual $MnFe_2O_4$ particles were magnetic,

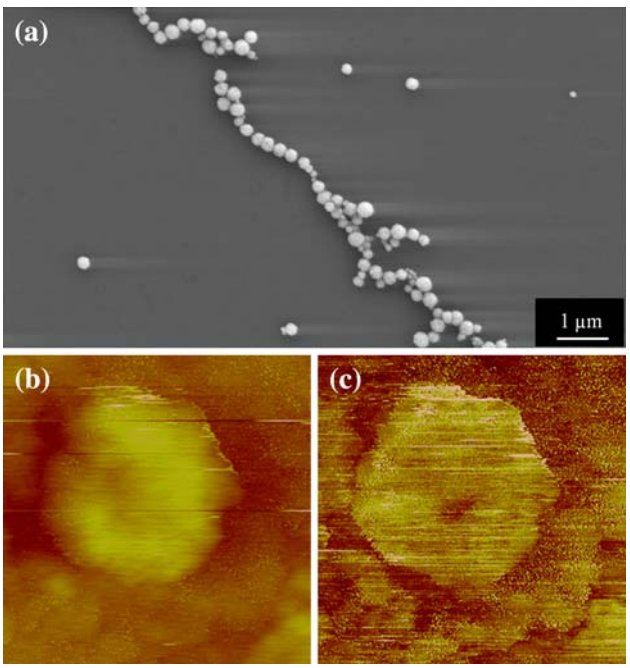

Fig. 2 **a** SEM image, **b** AFM image, and **c** MFM image of $MnFe_2O_4$ particles onto a glass substrate

which shows MFM images obtained from monolayer, spread onto a glass substrate.

The zeta-potentials for the $MnFe_2O_4$ particles were found to be in the range of +40 mV to −40 mV for $2 \leq pH \leq 12$ (see Fig. 1b). Higher negative surface charges, such as the particles for $pH > 10$, were used as a driving force to coat Ni onto the $MnFe_2O_4$ particles. In the alkaline conditions, Ni^+ ions dissociating from $NiCl_2$ and $NiSO_4$ interact with the negatively charged $MnFe_2O_4$ particles. Figure 3a shows SEM images of Ni-coated $MnFe_2O_4$ particles that were synthesized in the pH range of 2–12. The Ni content in the $MnFe_2O_4$–Ni composite particles increased from a total weight percentage of 0.6–6.3 wt% for $8 \leq pH \leq 11$, as shown in Fig. 3b. Table 1 lists the measured composition using EDS analysis. The results of Fig. 3 were utilized to identify the optimum solution process conditions, and indicate how the metal–shell thickness ratio can be controlled by varying the pH. The adhesion between the metal and ceramic was found to be quite good as further processing did not indicate any changes in the morphology. Figure 4 shows the magnetic properties of $MnFe_2O_4$–Ni core–shell particles. At room temperature, the saturation and remanent magnetization of core–shell particles were found to decrease by 43% and 50% with respect to that of core. The decrease in magnetization can be associated with the low value of these quantities for nickel. The core–shell particles were found to have the coercivity of 100 Oe, similar to that of core particles.

Figure 5a, b shows TEM images of the $MnFe_2O_4$ particles before and after Ni coating. The core–shell particles in Fig. 5b were synthesized under a $pH = 11$. Figure 5c shows a high-resolution TEM image for a $MnFe_2O_4$–Ni core–shell particle. This image reveals that Ni shells uniformly coat onto $MnFe_2O_4$ particles with a thickness of 1 nm. EDS analysis conducted at point 2 (marked in Fig. 5c) revealed a higher Ni concentration as compared to Fe, than that at point 1. This confirms that the Ni coating was limited to the surface of the $MnFe_2O_4$ particles with almost no interdiffusion. Figure 6 shows selected area electron diffraction patterns for (a) $MnFe_2O_4$ particles and (b) $MnFe_2O_4$–Ni core–shell particles. Additional rings from Ni can be seen in the diffraction pattern of core–shell particles. Rings from (111) and (200) of Ni were indexed for the Ni-coated $MnFe_2O_4$ particles. Thus, by combining the results of Figs. 5 and 6, we can confirm the uniform coating onto the $MnFe_2O_4$ particles.

Conclusion

In summary, $MnFe_2O_4$–Ni core–shell particles were synthesized by an aqueous method with shell-thickness

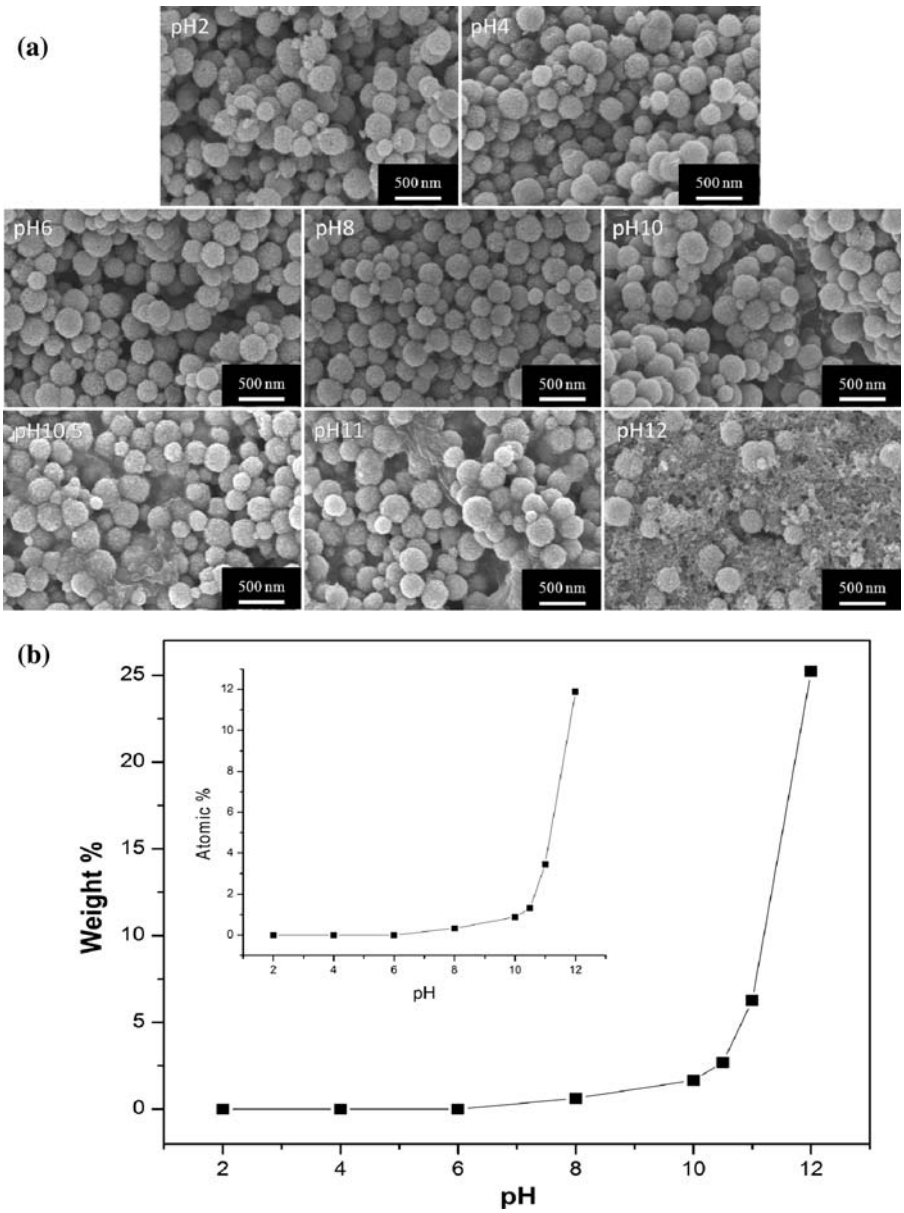

Fig. 3 **a** SEM images and **b** Ni contents of $MnFe_2O_4$–Ni core–shell particles synthesized for $2 \leq pH \leq 12$

Table 1 Weight percent (wt%) and atomic percent (at.%) of Ni element of $MnFe_2O_4$–Ni core–shell particles

pH	wt%	at.%
2.0	0	0
4.0	0	0
6.0	0	0
8.0	0.62	0.32
10.0	1.67	0.88
10.5	2.69	1.30
11.0	6.26	3.46
12.0	25.22	11.89

controlled in the range of 1 nm. The $MnFe_2O_4$ core particles were found to have a saturation magnetization of 74 emu/g and a coercivity of 89 Oe. HR-TEM and SAED

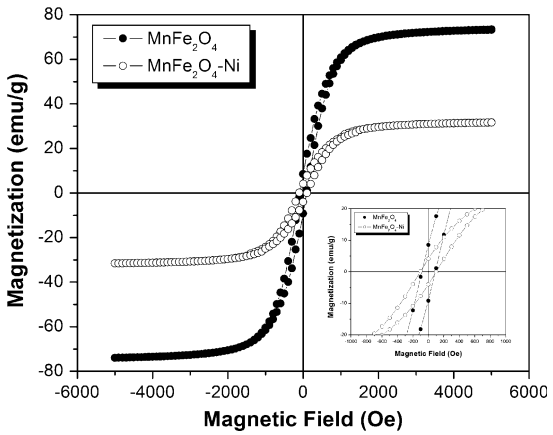

Fig. 4 M–H curves of $MnFe_2O_4$ and $MnFe_2O_4$–Ni particles

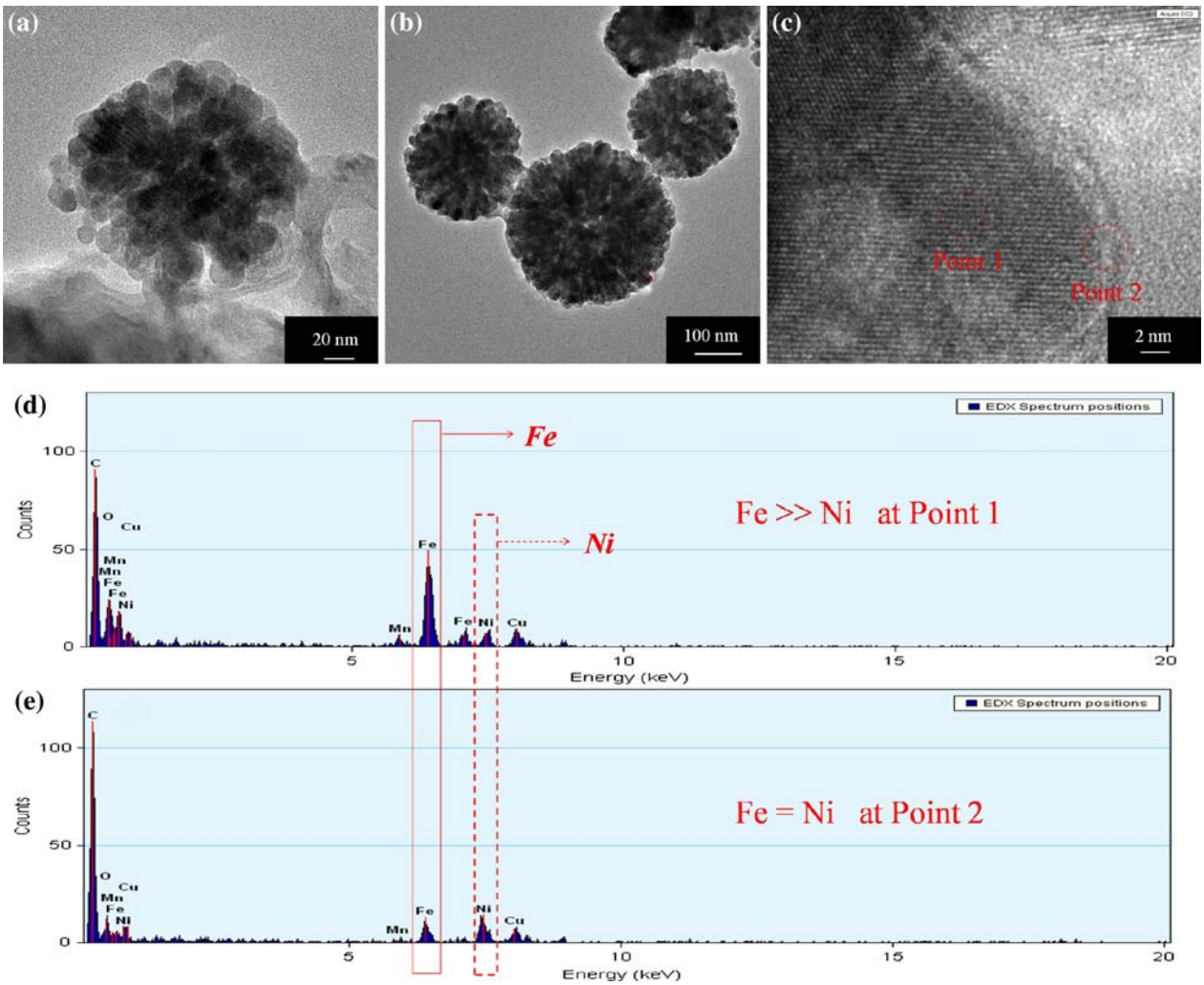

Fig. 5 TEM images of **a** $MnFe_2O_4$ particles and **b** $MnFe_2O_4$–Ni core–shell particles, **c** HR-TEM image of $MnFe_2O_4$–Ni core–shell particles, **d** EDS at Point 1 of $MnFe_2O_4$–Ni core–shell particles, and **e** EDS at Point 2 of $MnFe_2O_4$–Ni core–shell particles

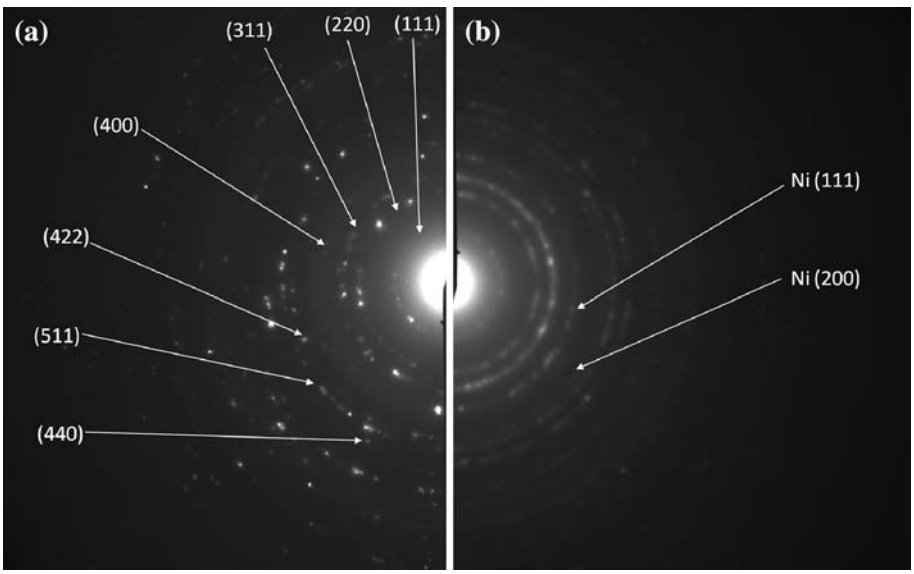

Fig. 6 Selected area electron diffraction patterns of **a** $MnFe_2O_4$ particles and **b** $MnFe_2O_4$–Ni core–shell particles

analyses were used to identify that the Ni shells had been successfully coated onto $MnFe_2O_4$ core particles with a uniform thickness.

Acknowledgement The authors gratefully acknowledge the financial support from National Science Foundation.

References

1. Bate G (1991) J Magn Magn Mater 100:413
2. Sugimoto M (1999) J Am Ceram Soc 82:269
3. Liu C, Zou BS, Rondinone AJ, Zhang ZJ (2000) J Phys Chem B 104:1141
4. Groman EV, Bouchard JC, Reinhardt CP, Vaccaro DE (2007) Bioconjugate Chem 18:1763
5. Dong SX, Zhai JY, Li JF, Viehland D, Priya S (2008) Appl Phys Lett 93:103511
6. Jiao J, Seraphin S, Wang XK, Withers JC (1996) J Appl Phys 80:103
7. Patton ST, Bhushan B (1998) IEEE Trans Magn 34:575
8. Guan S, Nelson BJ, Vollmers K (2004) J Electrochem Soc 151:C545
9. Lupi C et al (2005) Smart Mater Struct 14:N71
10. Athanassiou EK, Grass RN, Stark WJ (2006) Nanotechnology 17:1668
11. Tan FY, Fan XB, Zhang GL, Zhang FB (2007) Mater Lett 61:1805
12. Deng H et al (2005) Angew Chem-Int Edit 44:2782